

Performance of a TiN-coated monolithic silicon pin-diode array under mechanical stress

B. A. VanDevender^{*,1}, L. I. Bodine, A. W. Myers¹,
J. F. Amsbaugh, M. A. Howe², M. L. Leber³, R. G. H. Robertson,
K. Tolich, T. D. Van Wechel, B. L. Wall

*Center for Experimental Nuclear Physics and Astrophysics, and Department of
Physics, University of Washington, Seattle, WA 98195, USA*

Abstract

The Karlsruhe Tritium Neutrino Experiment (KATRIN) will detect tritium beta-decay electrons that pass through its electromagnetic spectrometer with a highly-segmented monolithic silicon *pin*-diode focal-plane detector (FPD). This *pin*-diode array will be on a single piece of 500- μm -thick silicon, with contact between titanium nitride (TiN) coated detector pixels and front-end electronics made by spring-loaded pogo pins. The pogo pins will exert a total force of up to 50 N on the detector, deforming it and resulting in mechanical stress up to 50 MPa in the silicon bulk. We have evaluated a prototype *pin*-diode array with a pogo-pin connection scheme similar to the KATRIN FPD. We find that pogo pins make good electrical contact to TiN and observe no effects on detector resolution or reverse-bias leakage current which can be attributed to mechanical stress.

Key words: silicon, *pin* diode, mechanical stress, leakage current, titanium nitride, pogo pin.

PACS: 29.40.Gx, 29.40.Wk

* Corresponding author. brent.vandevender@pnnl.gov

¹ Present Address: Pacific Northwest National Lab, Richland, WA 99354, USA

² Present Address: Department of Physics, University of North Carolina, Chapel Hill, NC 27599, USA

³ Present Address: Department of Physics, University of California, Santa Barbara, CA 93106, USA

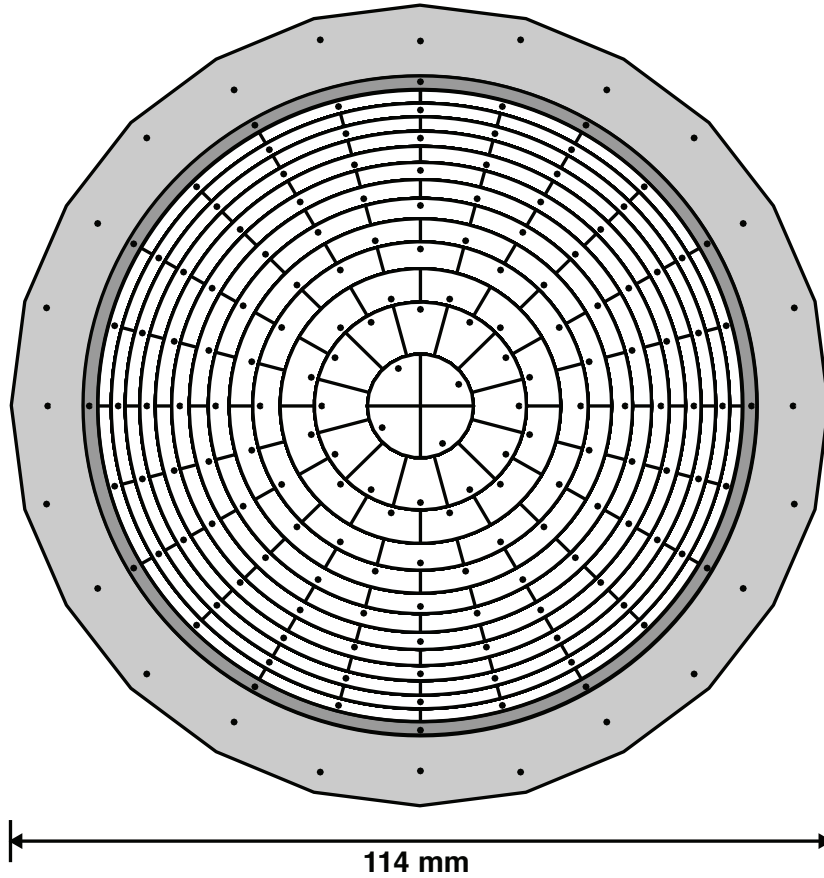


Fig. 1. KATRIN FPD, viewed from the pixelated (back) side. Lighter gray fill at the edge denotes the bias region which wraps around to the opposite side. Darker gray fill denotes the guard ring. White fill denotes individual *pin*-diode pixels. Dots denote points on the device that are contacted by pogo pins. See text for details.

1 Introduction

2 The Karlsruhe Tritium Neutrino Experiment (KATRIN) is a direct, model-
 3 independent search for the absolute mass of the electron antineutrino [1]. The
 4 highest energy electrons from the beta decay of molecular tritium (T_2) will be
 5 selected by a MAC-E spectrometer [2] and tagged with a focal-plane detector
 6 (FPD). The overall sensitivity to antineutrino mass depends critically on the
 7 minimization of backgrounds, which can be achieved by placing the FPD in
 8 extreme high vacuum (XHV) ($p \sim 10^{-9}$ Pa) and avoiding materials with high
 9 natural radioactivity near the FPD. These conditions constrain the design of
 10 the FPD and preclude many standard detector construction materials and
 11 techniques. Therefore we have developed a novel scheme to support and read
 12 out the FPD.

13 The KATRIN FPD (Fig. 1) is a monolithic silicon *pin*-diode array manufac-
14 tured by Canberra, Belgium. The *n*-type silicon substrate wafer is 500 μm
15 thick with a diameter of 114 mm. It is bare, with no housing or backing of any
16 kind. The entrance, or front side, is uniformly n^{++} -doped with no segmenta-
17 tion. The back side is p^{++} -doped in 148 individual 44.1-mm² pixels arranged
18 in a circular dartboard pattern surrounded by a continuous guard ring. The
19 $\langle 111 \rangle$ crystal orientation is perpendicular to the surface. The outermost pix-
20 els extend to a diameter of 90 mm. A guard ring extends from a diameter of
21 90 mm out to 94 mm. The pixels and guard ring are covered with titanium ni-
22 tride (TiN) for electrical contact to the front-end electronics. The guard ring
23 is to be held at signal reference potential to sink surface currents that might
24 otherwise flow between the outer pixels and regions of the surface held at bias
25 potential. Outside the guard ring there is a coating of TiN (but no doping)
26 from a diameter of 100 mm extending around the edge of the wafer to the n^{++}
27 doping on the front side. The TiN on the front side extends a few mm from
28 the edge, but the front is otherwise unmetallized. This configuration allows
29 the bias potential on the front side to be applied via connections made on the
30 back side adjacent to signal connections. TiN was chosen as a coating over
31 more commonly used metals such as aluminum because it is non-oxidizing.
32 The resistance of thin oxide layers is likely to have prevented good electrical
33 contact to the front-end electronics. Silver, though nonoxidizing, is excluded
34 because it would create a background from an atomic fluorescence near in
35 energy to the highest energy T_2 beta-decay electrons of interest to KATRIN.

36 The radiopurity requirements also limit the choice of techniques for connecting
37 the detector to its front-end electronics. In particular, wire bonding is avoided
38 because of the radioactivity of ceramic substrates typically used in the process.
39 The process of bonding ceramic to silicon can also create localized regions
40 of very high stress because of dissimilar coefficients of thermal expansion.
41 Instead, the connection between detector and electronics is made by an array of
42 spring-loaded pogo pins. The pins are manufactured by Interconnect Devices,
43 Inc. (item SS-30 with tip option J). They are made of inherently radiopure and
44 XHV-compatible materials. The FPD is supported at a diameter of 99 mm on
45 its front side while the pins press into the TiN on the back side. The front-
46 end electronics are on the opposite side of a feedthrough in a region of high
47 vacuum ($p \sim 10^{-5}$ Pa).

48 There will be a total of 184 pins pushing on the FPD; one for each of the 148
49 pixels, 12 contacting the guard ring and 24 applying bias to the outermost ring.
50 These pins will exert a total force of up to 50 N on the FPD, which will deform
51 it, causing mechanical stress up to 50 MPa in the silicon bulk. Mechanical
52 stress reduces the band gap energy in silicon and thus increases the bulk-
53 generated reverse-bias leakage current through a *p/n* junction with respect
54 to unstressed silicon [3]. In this model, 50 MPa of stress in the region of the
55 junction causes approximately 25% increase in leakage current. Stress can also

56 induce an increase of approximately 10% in junction capacitance for p^+/n and
57 n^+/p junctions under a few volts of reverse bias [4]. Both effects would tend to
58 degrade the energy resolution of a silicon *pin*-diode detector by several percent,
59 if they apply to such devices. Most troubling for KATRIN is a report [5]
60 demonstrating that stress causes leakage current to increase by up to four
61 orders of magnitude in a few specimens of outer silicon tracker sensors at the
62 Large Hadron Collider’s Compact Muon Solenoid (CMS). No mechanism for
63 this correlation is proposed, though bulk defects in the silicon are ruled out as
64 the cause. The behavior was observed only in a small subset of the production
65 line CMS devices from one of two manufacturers. Prototypes from the same
66 manufacturer did not show the correlation. The mechanisms described in [3]
67 can not account for such large increases. Order-of-magnitude leakage-current
68 increases are predicted for stressed small-pitch devices [6], though it seems
69 unlikely that that model would apply to some but not all of the CMS devices.

70 It is not clear whether the expected mechanical stress would cause similar
71 behavior in the KATRIN FPD. In this work, we demonstrate the efficacy
72 of the KATRIN FPD connection scheme by implementing it on a prototype
73 *pin*-diode array similar to the FPD in dimensions and doping architecture.
74 Properties of this detector are measured while unstressed and for a range of
75 pogo-pin applied stresses up to a maximum of 30–42 MPa. No stress-induced
76 effects on the detector performance are observed.

77 2 Detector and Apparatus

78 Canberra, Belgium provided a prototype *pin*-diode array for evaluation (Fig. 2).
79 The prototype’s doping architecture is identical to that of the FPD except that
80 the prototype has a thicker n^{++} layer on the entrance side and its window is
81 metalized with aluminum. Like the FPD, the prototype array is monolithic on
82 a 500- μm -thick silicon wafer with the $\langle 111 \rangle$ crystal orientation perpendicular
83 to the surface. The back side is also coated with TiN for ohmic contact to the
84 pixels. The wafer measures 127 mm in diameter and has 158 8- mm^2 pixels. The
85 apparatus constructed for these tests allows for measurements of the proto-
86 type’s basic *pin*-diode detector properties under controlled applied loads from
87 a pogo-pin array. The pogo-pin array is lowered from above. The entrance side
88 of the detector faces down towards a sealed 10- μCi ^{241}Am source, placed 6.4 cm
89 below the detector. Preamplifiers are mounted above the pogo-pin array. The
90 entire apparatus resides inside an electrically-shielded light-tight enclosure.

91 The detector is held firmly between two Delrin rings with inner diameters
92 of 110 mm. A ring of electrically conductive elastomer sits between the lower
93 ring and the detector in a recess cut into the Delrin. The recess is slightly
94 shallower than the thickness of the uncompressed elastomer so that when the

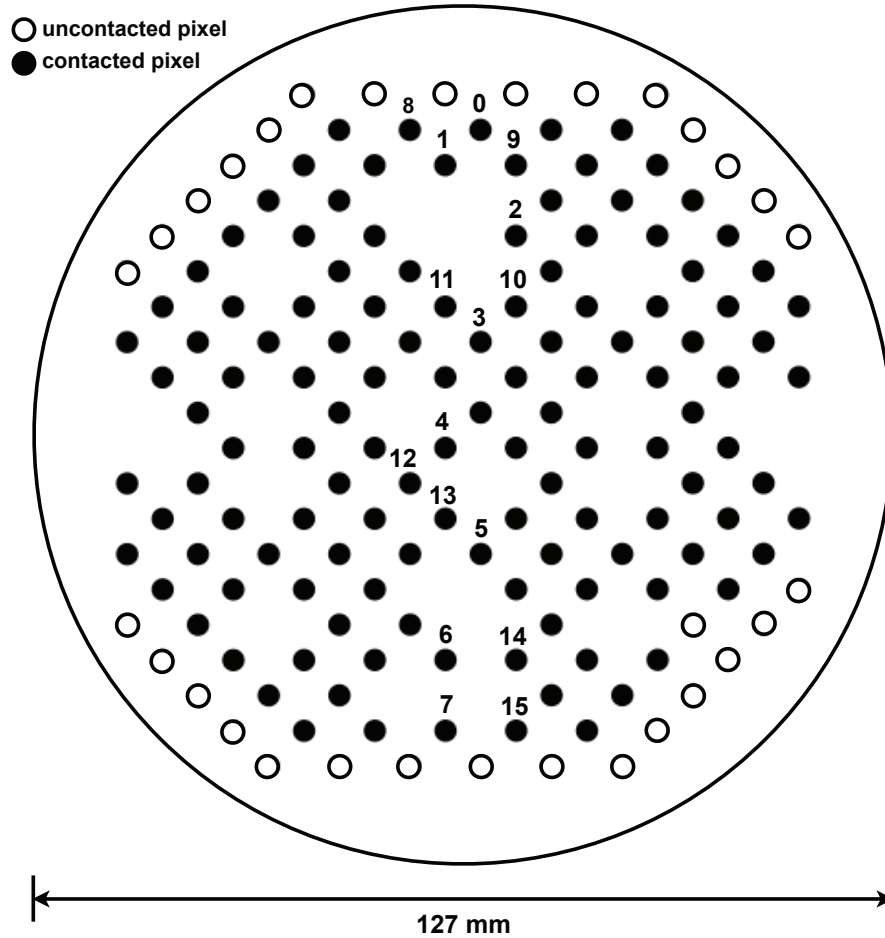


Fig. 2. Pixel layout of the prototype *pin*-diode array used for these measurements, viewed from the pixelated side. Solid circles are TiN-coated actively doped *pin*-diode regions which are contacted by pogo pins. Open circles are TiN-coated actively doped *pin*-diode regions which are not contacted by pogo pins. All pogo pins contact at the center of a diode region. The numbers 0–15 appear just above the sixteen channels instrumented for these measurements. See text for details.

95 upper ring is attached the elastomer is compressed for good electrical contact
 96 to the detector. The recess extends to the outer edge of the holder in eight
 97 channels. Positive bias potential is applied to the detector via wires pinched
 98 between the elastomer and the upper Delrin ring in each of these channels.
 99 For control measurements of the detector’s performance with no stress, an
 100 additional plug of Delrin and elastomer is inserted to support the detector
 101 from below the front side. The apparatus is shown in Fig. 3.

102 Electrical contact to each pixel is made by a spring-loaded conducting pogo
 103 pin. The pins are manufactured by Interconnect Devices, Inc. (item number
 104 SS30 with a rounded tip [option J] and a stainless steel spring). Each pin is
 105 preloaded such that it takes a force of 0.137 N to initiate any compression of
 106 the plunger and an additional force of 0.133 N per 1000 μm of compression.

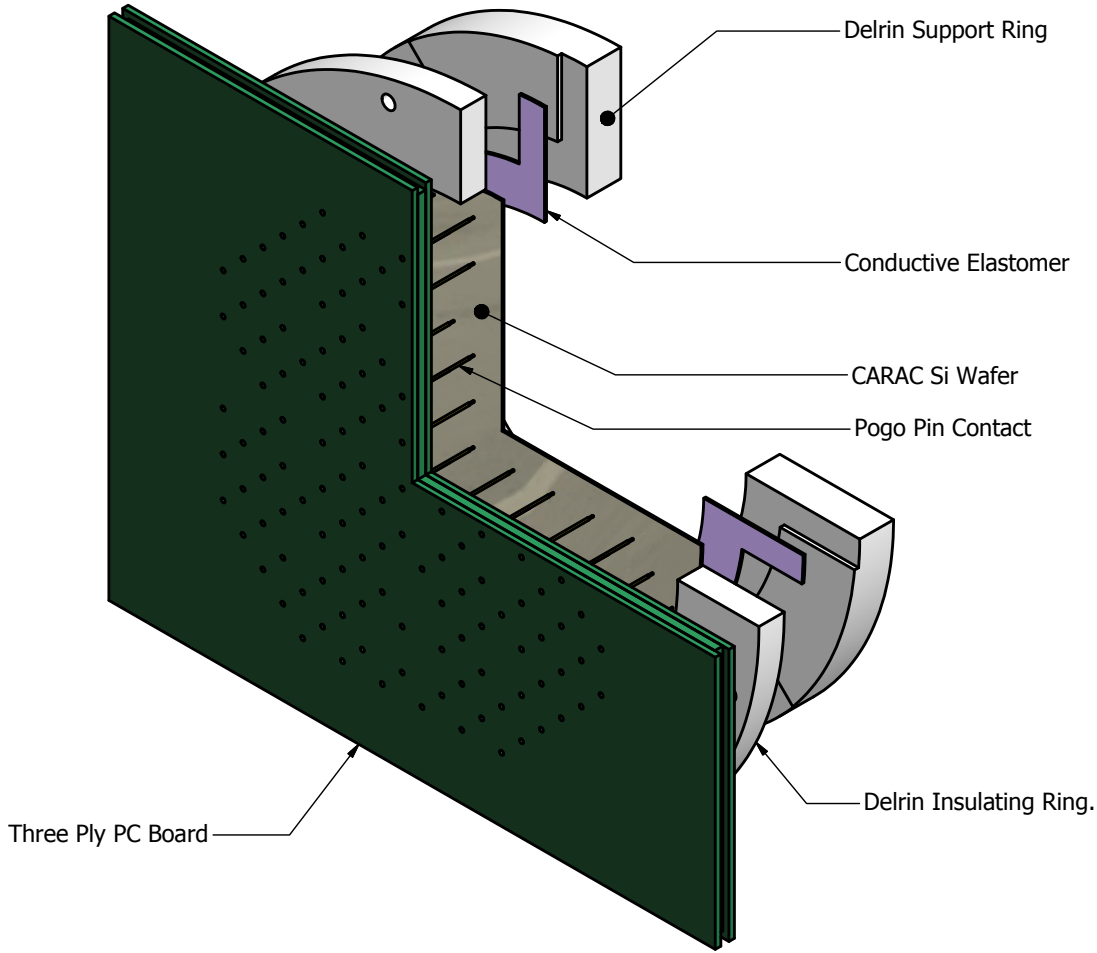


Fig. 3. An exploded cut-away view of the prototype apparatus.

107 The pogo-pin array is aligned with the detector such that each pin contacts
 108 the center of one pixel. Close mechanical tolerances between the array and
 109 the detector holder preclude contacting 30 of the outermost pixels, and one
 110 interior pin was damaged during construction of the apparatus, leaving a total
 111 of 127 pogo pins applying force to the detector. The pins are mounted and
 112 soldered into a stack of five 1.57-mm-thick FR4 circuit boards which is much
 113 more rigid than the detector. The pins are positioned such that the variation
 114 in the relaxed vertical position of the tips is less than $25\ \mu\text{m}$. A micrometer sets
 115 the pogo-pin array translation with an accuracy of $25\ \mu\text{m}$, up to a maximum
 116 of $1020\ \mu\text{m}$ with respect to initial detector contact.

117 Uniformity of the applied load is ensured through precise alignment of the
 118 pogo-pin array relative to the detector. The height of all surfaces nominally
 119 parallel to the detector deviates less than $25\ \mu\text{m}$, even under the maximum
 120 loads allowed by the apparatus. A blank silicon wafer with identical dimen-
 121 sions as the prototype detector was installed into the apparatus. Fig. 4 shows
 122 the displacement of the center of the blank wafer and the smaller deflection

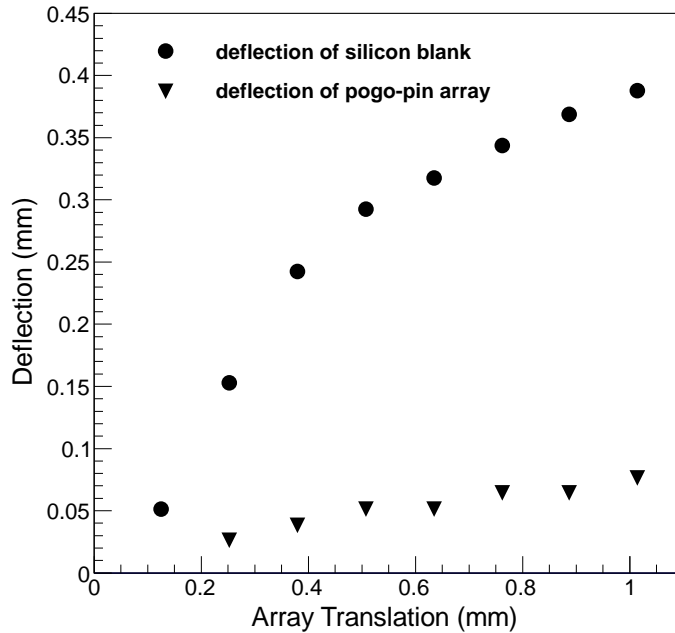


Fig. 4. Mechanical performance of the apparatus with a blank silicon wafer installed. The abscissa is the distance which the base of the pogo-pin array has translated since initial contact with the detector.

123 of the center of the pogo-pin array caused by the reaction force. Due to these
 124 deflections, care must be taken to ensure that all pins are compressed at least
 125 to the manufacturer's specification of $380\ \mu\text{m}$ because electrical contact is in-
 126 consistent when the pins are under-compressed. The array must be translated
 127 more than $760\ \mu\text{m}$ past initial contact with the detector so that pins near the
 128 center of the detector will meet the minimum requirement. As can be seen in
 129 Fig. 4, when the array is translated $760\ \mu\text{m}$, the pin compression in the center
 130 is reduced by the $340\ \mu\text{m}$ deflection of the detector in addition to the $60\ \mu\text{m}$
 131 deflection of the array itself, resulting in only $360\ \mu\text{m}$ compression of pins at
 132 the center.

133 3 Forces and Stress

134 Calculation of the total force on the detector by the entire array is complicated
 135 by the deformation of the detector under the applied load. The compression
 136 of each pin and deflection of the detector depend on the radial position in a
 137 way that is not exactly known. The more relevant quantity is the maximum
 138 stress in the detector, which can be estimated without knowing the total load,
 139 provided that the displacement d of the center of the detector is known (Fig. 4).
 140 Mechanically, our detector is a circular plate with fixed edges. The appropriate

141 relations are [7]:

$$142 \quad S = \frac{0.24W}{t^2} \text{ and } d = \frac{0.0543WR^2}{Et^3}, \quad (1)$$

143 where S is the maximum stress in the silicon, W is the total load, t is the
144 thickness of the detector, R is the radius of the supporting ring, and E is the
145 Young's modulus of silicon. The load, W , is trivially eliminated:

$$146 \quad S = \frac{0.24}{0.0543} \frac{dEt}{R^2}. \quad (2)$$

147 The Young's modulus of silicon ranges from 130–185 GPa, depending on the
148 crystal orientation with respect to the direction of applied stress. These for-
149 mulae are appropriate for uniformly distributed loads and deflections of less
150 than 50% of the plate thickness. However, the load on our detector has some
151 position dependence due to the variation in pogo-pin compression caused by
152 bowing of the detector, and our detector bows by 80% of its thickness under
153 the maximum load allowed by the apparatus (Fig. 4). Therefore we do not ex-
154 pect stresses calculated with equations (1) and (2) to be very precise, but take
155 them to be good estimates of the lower limit with the correct order of mag-
156 nitude. With these caveats in mind, equation (2) indicates that our detector
157 will have a maximum stress of 30–42 MPa at the maximum array translation
158 allowed by our apparatus. The stated range is due to the unknown orientation
159 of local stresses within the detector bulk.

160 4 Electronics

161 The custom-made charge-sensitive preamplifiers are prototypes of those to be
162 used for KATRIN. Because of limited availability of preamplifiers, only eight
163 pixels of the detector are tested simultaneously. A total of sixteen pixels were
164 tested in two separate series of measurements. They were chosen to give a rep-
165 resentative sample across a diameter of the detector. The stress is not uniform
166 throughout the volume, but the circular symmetry of the holder guarantees
167 that any stress depends only on the distance from the center of the detector.
168 During each pass, all pixels neighboring the eight active channels were held at
169 ground to ensure uniform electric fields in the active pixels and also to provide
170 an alternative path for any surface currents which might flow on the detector.
171 The ground connection was temporarily removed to test for stress-induced
172 surface currents. No difference was observed.

173 All of the leakage current through a detector pixel passes through a 5% pre-
174 cision 500 M Ω resistor on its preamplifier, adding a dc offset to the output

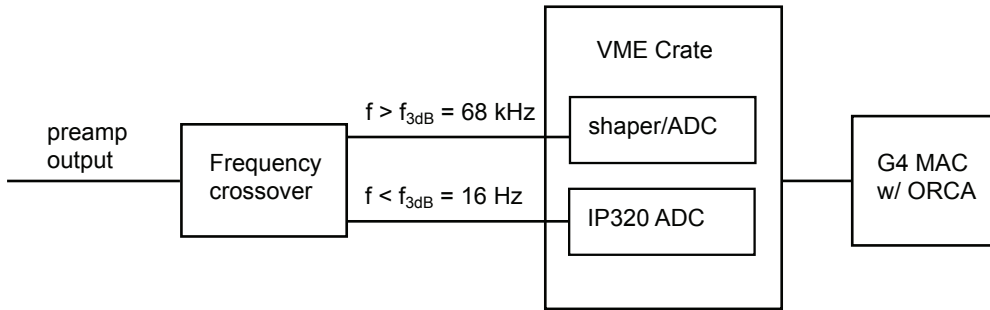


Fig. 5. Signal and data flow. The preamplifier outputs carry information about the energy of events in high frequency components while the dc component is proportional to the leakage current through the detector. The crossover segregates these frequency regimes so that they can be read out by appropriate devices.

175 signal. We compute the leakage current as the difference between the dc off-
 176 sets of the output signal when the detector is biased to V_{bias} and when it is
 177 floating at V_{float} with the bias supply physically disconnected, divided by the
 178 resistance:

$$179 \quad I_{\text{leak}}(V_{\text{bias}}) = [V_{\text{dc}}(V_{\text{bias}}) - V_{\text{dc}}(V_{\text{float}})] / 500 \text{ M}\Omega. \quad (3)$$

180 This relation was validated to an accuracy of $< 2\%$ using a picoammeter in
 181 series with the single bias supply such that it read the total current drawn by
 182 all eight instrumented channels. The picoammeter introduced a small amount
 183 of noise to the output signals, so it was removed during normal running con-
 184 ditions. The bias potential is $V_{\text{bias}} = 100 \text{ V}$ for all measurements reported
 185 here.

186 Detector outputs are split into two branches by a custom-made frequency
 187 crossover circuit. One branch carries components of the signal above a 3-
 188 dB cutoff frequency of 68 kHz into a VME-based shaper/ADC unit described
 189 in [8]. The dc offsets, V_{dc} , are carried on the other branch into an Acromag
 190 IP320A ADC housed in the same VME crate. Data are acquired from the
 191 VME crate by ORCA software [9] running on a Macintosh computer. The
 192 setup is shown schematically in Fig. 5.

193 The voltages on the dc lines are sampled once per second and these samples
 194 are then averaged during two-minute intervals. The measurements for each
 195 translation of the pogo-pin array consist of two such intervals – one to es-
 196 tablish $V_{\text{dc}}(V_{\text{float}})$ for every channel before the detector is biased and another
 197 to establish $V_{\text{dc}}(V_{\text{bias}})$ for every channel once the detector is at full bias. The
 198 statistical uncertainties in the leakage currents are due to the rms fluctuation
 199 of the sampled voltages. The resistor precisions are not taken into account
 200 since they affect all measurements with a given preamplifier by the same pro-

201 portion, and we are interested only in changes of the leakage currents. An
202 additional independent systematic uncertainty of ± 5 pA is added to account
203 for the temperature-dependent gate leakage of the FET at the preamplifier
204 input (see below).

205 5 Temperature Variations

206 The temperature of the apparatus is monitored but it is not controlled. The
207 temperature inside the light-tight enclosure is measured with a thermistor
208 mounted on the lower surface of the Delrin holder but exposed to air. The
209 temperatures of the detector and electronics are not directly measured. The
210 temperature is recorded at the beginning and end of each two-minute de-
211 offset sampling period. The nominal temperature for a single leakage current
212 measurement is the average of four readings, two for each of two sampling
213 periods. The nominal temperature range for the measurements presented here
214 is 24.4–25.6 °C, though the four individual values which determine any partic-
215 ular nominal temperature never differ by more than 0.1 °C. We assume that
216 fluctuations in the detector and electronics temperatures are the same size as
217 the fluctuations read on the thermistor. We therefore take the uncertainty in
218 the nominal temperature for each measurement to be 0.1 °C.

219 6 Results

220 Our results are demonstrated in two ways. The first examines the pulse-height
221 resolution of ^{241}Am gamma-rays as the stress in the detector is increased. The
222 second method is a direct measurement of leakage currents as discussed above.
223 Neither method reveals any effects attributable to the stress. The results are
224 qualitatively the same for all tested pixels. For brevity, we present results from
225 pixel 8 only.

226 Fig. 6 shows the raw ^{241}Am gamma-ray pulse-height spectra obtained with
227 seven different pogo-pin array translations from a typical pixel of our detec-
228 tor. The peak corresponding to the 59.5 keV gamma is labelled for reference.
229 The recognizable gamma-ray spectrum of ^{241}Am demonstrates the basic func-
230 tionality of our mounting scheme – the detector works under stress and the
231 pogo pins make good electrical contact to the TiN-coated pixels.

232 Fig. 7 shows the leakage current measurements from a typical pixel. The left
233 plot shows the leakage current versus the array translation, which corresponds
234 to increasing mechanical stress from left to right. The right plot shows the

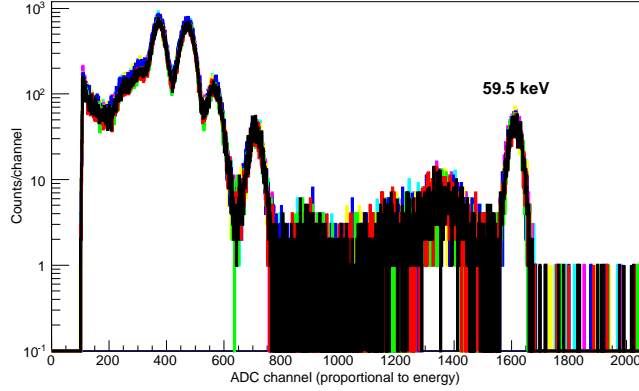


Fig. 6. The pulse-height spectra of ^{241}Am gamma rays from a single typical pixel for seven different translations of the pogo-pin array in steps of $130\ \mu\text{m}$ increasing from the initial compression of $380\ \mu\text{m}$. Different colors represent different translations. There is no statistically significant difference between these spectra.

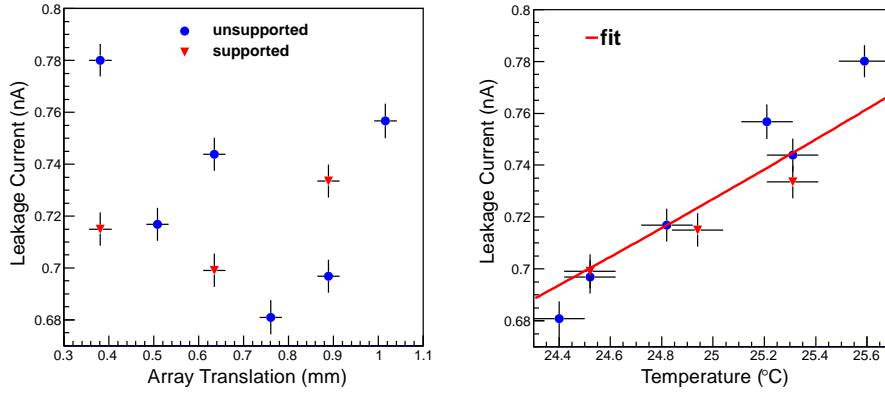


Fig. 7. Leakage current measurements from a typical pixel. Circles represent measurements taken on an unsupported detector. Triangles represent control measurements with the support in place. The left plot shows the leakage current versus the array translation. The right plot shows the same leakage current measurements versus the temperature at the time of the measurement. The data fit well with a function of the form of equation (4).

235 same leakage currents versus the temperature at the time they were mea-
 236 sured. Leakage currents in diode detectors are thermal in nature so it is neces-
 237 sary to account for temperature dependence when searching for stress-induced
 238 changes. The thermally generated leakage current I is proportional to the rate
 239 of electron-hole pair creation and is thus related to the absolute temperature
 240 T by [10]

$$241 \quad I(T) = NT^{3/2}e^{-E_g/2k_B T}, \quad (4)$$

242 where E_g is the bandgap energy and k_B is the Boltzmann constant. The nor-

malization N accounts for the device geometry and all factors contributing to charge-collection efficiency in the electronics (recombination etc.). The current measurements made with the detector unsupported are combined with those made with the detector supported and fit with a single function of the form (4), leaving the normalization N as the only free parameter. The data fit well ($p(\chi^2, \nu) = 0.07$), indicating that all observed variation in the current measurements can likely be attributed to the temperature dependence of bulk-generated leakage currents.

7 Conclusions

We have demonstrated the efficacy of a new mounting scheme for monolithic silicon *pin*-diode arrays. The scheme consists of contacting TiN coated pixels with an array of spring-loaded pins. We observed no measurable effects of the associated mechanical stress on the performance of our monolithic silicon *pin*-diode array for bulk stresses up to a few tens of MPa. The large leakage current increases reported in reference [5] were not observed in the sixteen tested pixels of our prototype detector. All observed effects can be attributed to temperature variations. The pogo-pin contact scheme to be used by KATRIN to connect its FPD to front-end electronics is not expected to have any problems related to the pin forces on the detector.

8 Acknowledgments

This research was supported by the US Dept. of Energy Division of Nuclear Physics through grant DE-FG02-97ER41020. The authors wish to thank Marijke Keters, Mathieu Morelle and the rest of their team at Canberra in Olen, Belgium for technical support of this research and for the design and fabrication of KATRIN FPDs.

References

- [1] J. Angrik et al., KATRIN Design Report, 2004. <http://www-ik.fzk.de/~katrin/publications/documents/DesignReport2004-12Jan2005.pdf>.
- [2] V.M. Lobashev and P.E. Spivak, Nuclear Instruments and Methods A 240 (1985) 305.
- [3] M. Furuhashi and K. Taniguchi, Journal of Applied Physics 103 (2008).

- [4] V. P. Gopinath et al., IEEE Electron Device Letters 23 (2002) 312.
- [5] A. J. Furgeri et al., Nuclear Instruments and Methods A 560 (2006) 108.
- [6] P. Smeys et al., IEEE Transactions on Electron Devices 46 (1999) 1245.
- [7] E. Oberg et al., Machinery's Handbook, 27th ed., Industrial Press Inc, 2004.
- [8] J.F. Amsbaugh et al., Nuclear Instruments and Methods A 579 (2007) 1054.
- [9] M.A. Howe et al., IEEE Transactions on Nuclear Science 51 (2004) 878.
- [10] G.F. Knoll, Radiation Detection and Measurement, 3rd ed., John Wiley and Sons, Inc., 2000.